Hindawi
International Journal of Aerospace Engineering
Volume 2019, Article ID 5151808, 12 pages
https://doi.org/10.1155/2019/5151808

Research Article

The Effect of Damping Coefficient, Spring Coefficient, and Mass Ratio on the Power Extraction Performance of a Semiactive Flapping Wing

Jianyang Zhu [1,2]

[1]*Institute of Robotics and Intelligent Systems, Wuhan University of Science and Technology, Wuhan 430081, China*
[2]*Hubei Key Laboratory of Mechanical Transmission and Manufacturing Engineering, Wuhan University of Science and Technology, China*

Correspondence should be addressed to Jianyang Zhu; zhujianyang02@163.com

Received 15 January 2019; Accepted 27 February 2019; Published 16 April 2019

Academic Editor: Gustaaf B. Jacobs

The effect of varying damping coefficient C^*, spring coefficient K^*, and mass ratio M^* on the semiactive flapping wing power extraction performance was numerically studied in this paper. A numerical code based on Finite Volume method to solve the two-dimensional Navier-Stokes equations and coupled with Finite Center Difference method to solve the passive plunging motion equation is developed. At a Reynolds number of 3400 and the pitching axis at quarter chord from the leading edge of the wing, the power extraction performance of the semiactive flapping wing with different damping coefficient, spring coefficient, and mass ratio is systematically investigated. The optimal set of spring coefficient is found at a value of 1.00. However, the variation of mass ratio M^* cannot increase the maximum mean power coefficient and power efficiency, but it can influence the value of damping coefficient C^* at which the wing achieves the maximum mean power coefficient and power efficiency. Moreover, insensitivity of the mean power coefficient and power efficiency to the variation of damping coefficient C^* is observed for the wing with smaller mass ratio, which indicates the wing with smaller M^* has better working stability.

1. Introduction

The application of flapping wing for energy extraction is inspired by insects and birds, who exhibit excellent aerodynamic performance by extracting wind energy through flapping their wings. Comparing to the conventional rotation energy extraction turbines, flapping wing power generator possesses many advantages, such as simpler design, less construction costs, more efficiency in low stream speeds, and more friendly to the flying creatures in nature [1]. Therefore, more and more recently researches have been focused on this type of power generator [2–5].

Up to now, there are three types of flapping wing power generator, named fully active [6], semiactive, and purely passive system, respectively [7]. Among them, the semiactive flapping wing power generator which has one of the flapping motion (pitching) is actuated and another motion (plunging) is induced by free stream fluid and is considered as a more feasible approach in industry, because it is easy to implement and control [8, 9]. This type of flapping wing power generator is characterized by the interaction coupling of fluid, driven wing pitching, and passive wing plunging, which results the flow around the generator very complex, and the energy extraction performance is still the main research focus of this type of power generator.

To investigate the energy extraction performance of a semiactive flapping wing near solid walls, the mechanical parameters of the wing to achieve power extraction efficiency were optimized by Wu et al. [10]. They concluded that the spring constant at a value of 1.0 and damping coefficient at a value of π are an optimal choice to achieve net power extraction efficiency of the wing, when the wing has fixed wing mass at a value of 1.0 and Reynolds number at a value of 1100. Under the same Reynolds number, Zhan et al. [11] performed a similar numerical study to optimize the energy extraction performance of a semiactive flapping wing with

fixed wing mass at a value of 1.0 and reduced frequency $f^* = 0.2$. It was found that the parameters for the wing that achieved best power extraction are the difference with different pitching amplitude. For the wing with pitching amplitude $\theta_m \leq 67.5$, the optimal power extraction efficiency is achieved when the wing has the spring constant at a value of 5.0 and damping coefficient at a value of π, while for the wing with pitching amplitude $\theta_m > 67.5$, the optimal power extraction efficiency is achieved when the wing has the spring constant at a value of 5.0 and damping coefficient at a value of 0.5π. Moreover, based on the numerical study by Zhu et al. [12], the optimal power extraction performance is the system where there is no spring on the plunge motion and the damping coefficient is at a value of π.

On the other hand, to explore an inertial effect on the power extraction performance of a semiactive flapping wing, Deng et al. [13] conducted a strong fluid-structure coupling method to study the power extraction performance of a semiactive flapping wing with different mass ratios (ranging from 0.125 to 100), and it was found that the energy harvesting efficiency decreases monotonically with increasing mass ratio. However, the amount of power extraction changes very little when the wing has mass ratio less than 10. While, according to the experiment study on a flapping wing hydroelectric power generation system by Abiru and Yoshitake [14], the wing with lager mass ratio is needed to excite the hydroelastic response; therefore, the wing with lager mass ratio has better power extraction performance.

As discussed above, the effect of damping coefficient, spring constant, and mass ratio on the power extraction performance of the semiactive flapping wing is still not clearly understood. Therefore, in this paper, a numerical code based on Finite Volume method to solve the two-dimensional Navier-Stokes equations and coupled with Finite Center Difference method to solve passive plunging motion equation is employed. The flow around a semiactive flapping wing is simulated with different damping coefficient, spring constant, and mass ratio. The NACA0015 airfoil is employed to represent the two-dimensional section wing, and the power extraction performance as well as the fluid around the wing are studied details in the following.

2. Problem Definition and Methodology

2.1. Problem Definition. In this paper, NACA0015 airfoil with chord length d and mass M is employed to model the flapping wing. A damper with damping coefficient C and spring constant K which is attached to the wing is employed to mimic the power extractor. The schematic view of the semiactive flapping wing is shown in Figure 1, where the profile $\theta(t)$ is defined to drive the pitching motion of the wing; the plunging motion $h(t)$ is induced by the lift force of the wing. The pitching point O is located at the center line of the wing with a distance $0.25d$ from the leading edge. To simplify the problem, a cosine pitching motion mode is employed, and the center of mass of the wing is also designed to coincide with the pitching point O. Then, the governing equation of

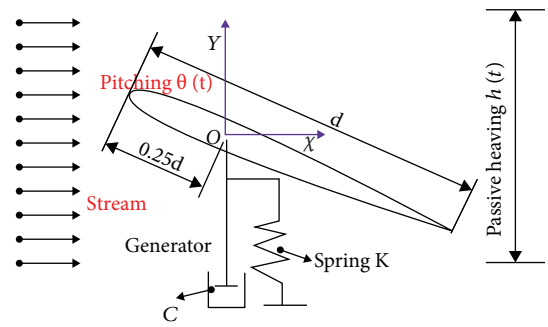

Figure 1: The schematic view of the semiactive flapping wing.

the pitching motion $\theta(t)$ and passive plunging motion $h(t)$ can be defined as

$$\theta(t) = -\theta_m \cos(2\pi f t), \tag{1}$$

$$M\ddot{h} + C\dot{h} + Kh = F_L, \tag{2}$$

where θ_m is the pitching amplitude, f is the pitching frequency, F_L is the lift force in Y direction as shown in Figure 1. The left and right sides of equation (2) is divided by the mass, then, it can be described as

$$\ddot{h} + \frac{C}{M}\dot{h} + \frac{K}{M}h = \frac{F_L}{M}. \tag{3}$$

It is seen from equation (1) to equation (3) that if we fix the pitching amplitude θ_m and pitching frequency f, the kinematic of the semiactive flapping wing is determined by the following three characteristic parameters:

$$C^* = \frac{C}{M},$$
$$K^* = \frac{\sqrt{K/M}}{(2\pi f)}, \tag{4}$$
$$M^* = \frac{\rho_s d}{\rho d},$$

where ρ is the fluid density, ρ_s is the wing density, $M = \rho_s S$, and S is the area of the wing. Moreover, the Reynolds number Re and reduced frequency f^* can be defined as

$$\mathrm{Re} = \frac{\rho U_\infty d}{\mu},$$
$$f^* = \frac{2\pi f d}{U_\infty}, \tag{5}$$

where U_∞ is the stream velocity and ν is the fluid kinematic viscosity.

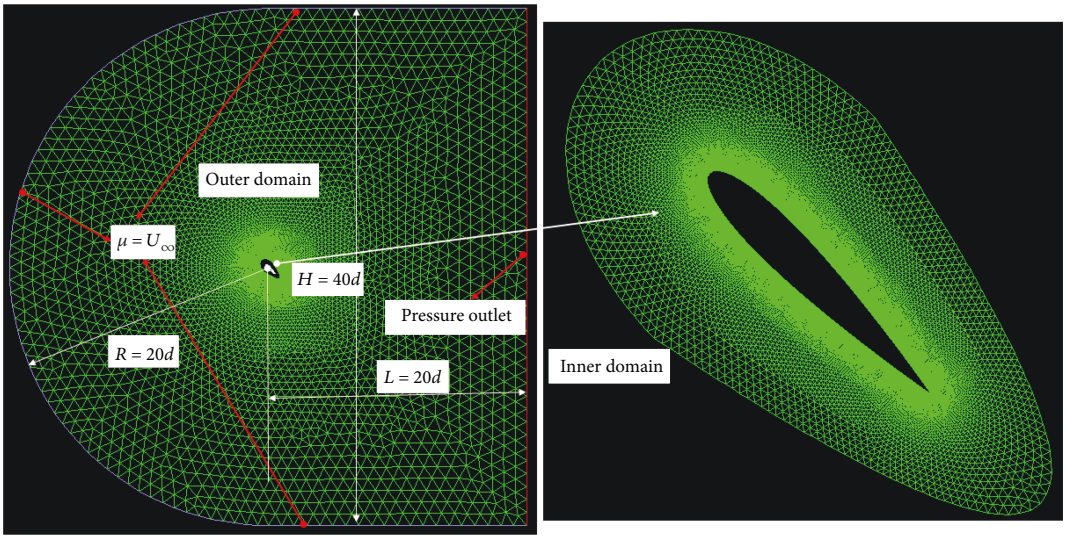

Figure 2: Schematic of the computational grid and boundary conditions.

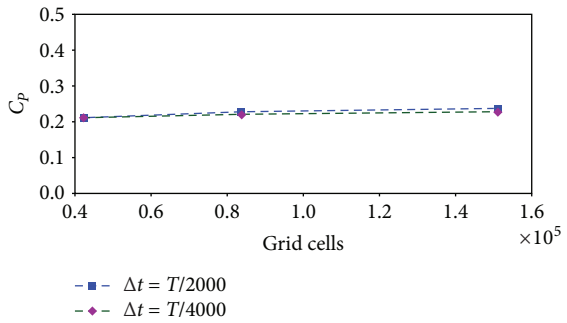

Figure 3: The power coefficient of a semiactive flapping wing with different meshes and iteration time steps.

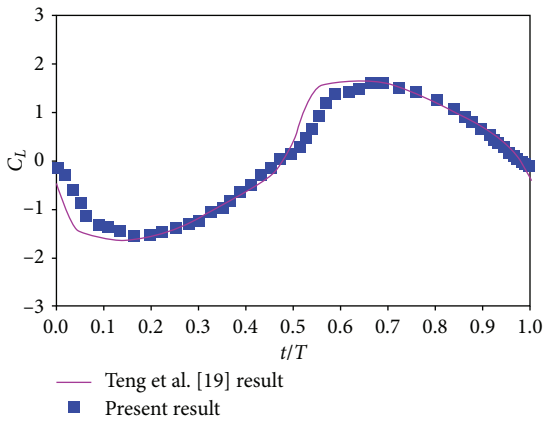

Figure 4: The lift coefficient of a semiactive flapping wing.

When the semiactive flapping wing is working, the power extracted from the fluid can be described as

$$P_E = C\dot{h}^2, \tag{6}$$

and the power which is needed to input the system to drive the pitching motion can be described as

$$P_I = -M_T\omega, \tag{7}$$

where M_T is the fluid torque about the pitching axis O and ω is the pitching velocity. Then, the net power is given by

$$P_T = P_E - P_I, \tag{8}$$

and the power coefficient is described as

$$C_P = \frac{P_T}{0.5\rho U_\infty^3 d}. \tag{9}$$

Table 1: Parameters considered in this paper.

Damping coefficient C^*	Spring coefficient K^*	Mass ratio M^*
0.0625~18.0	0.00~3.00	15~240

The mean energy coefficient can be defined as

$$\overline{C_P} = \frac{1}{T}\int_t^{t+T} C_P dt, \tag{10}$$

where T is the pitching period.

Then, the power extraction efficiency of the generator can be defined as

$$\eta = \frac{\overline{P_T}}{0.5\rho U_\infty^3 h_{\max}} = \overline{C_P}\frac{d}{h_{\max}}, \tag{11}$$

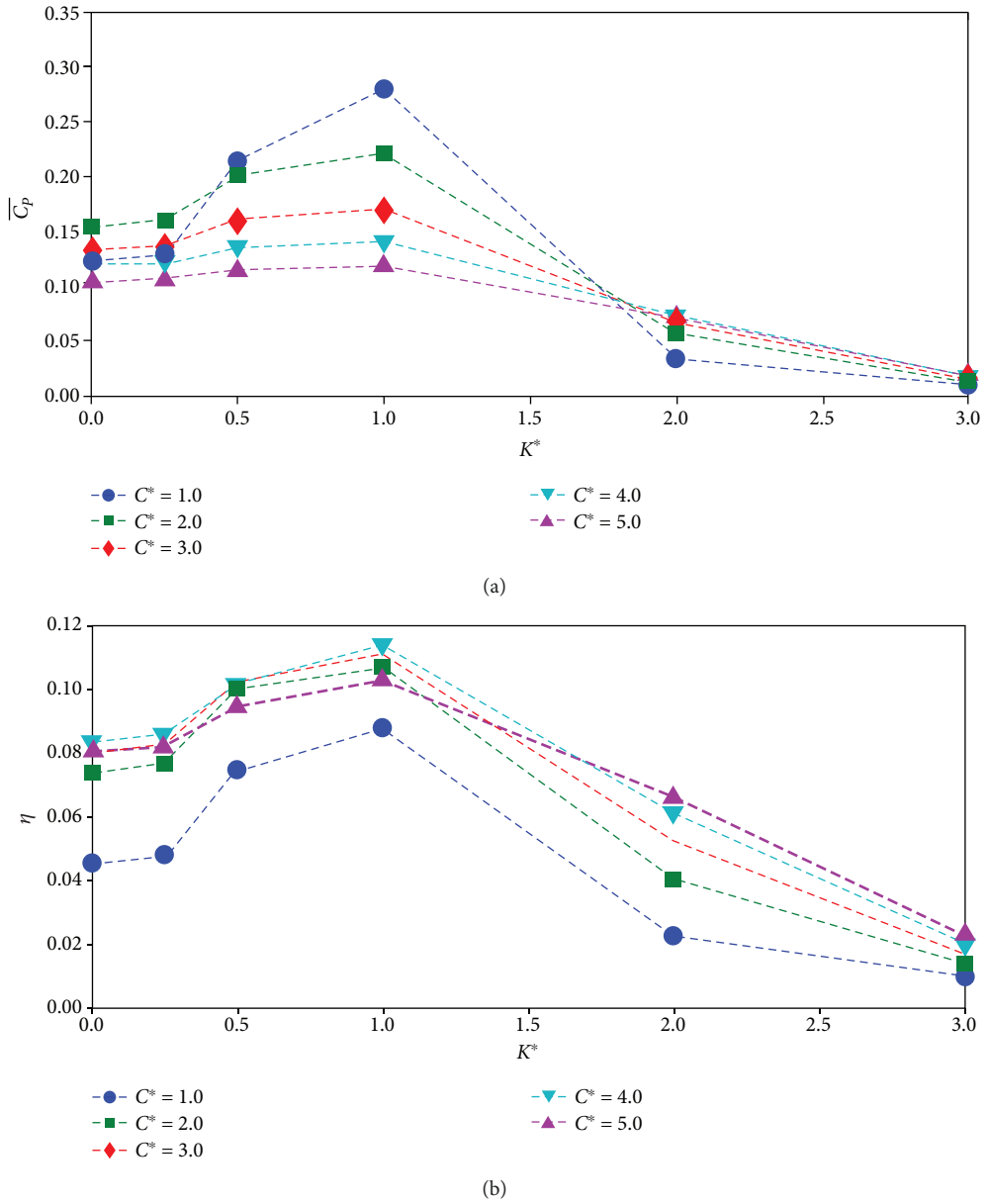

FIGURE 5: The mean power coefficient and power efficiency against spring coefficient K^* with different damping coefficient C^*; (a) mean power coefficient; (b) power efficiency.

where $h_{\max}$ is the overall vertical extent of the wing motion (the distance in Y direction between the highest position and the lowest position reached by the wing, either the leading edge or the trailing edge). It is defined as the maximum value of the following equation:

$$h_{\max} = \max\left(\text{amplitude}(h + 0.75d\sin(\theta)), \text{amplitude}(h - 0.25d\sin(\theta))\right). \quad (12)$$

Note that the drag force has not been mentioned in this work, because it does not contribute to the power production.

2.2. Numerical Method. Based on the free stream velocity and the chord length of the wing, the Reynolds number and Mach number are fixed at a value of 3400 and 0.0015, respectively. According to our previous work [5], at Reynolds number 3400, the flow assuming laminar, the calculating results can match experimental results very well for flapping wing. Therefore, the fluid around the wing is assumed as laminar and incompressible. The governing equation can be described as

$$\nabla \cdot V = 0, \quad (13)$$

$$\frac{\partial V}{\partial t} + V \cdot \nabla V = -\frac{1}{\rho}\nabla p + \frac{\mu}{\rho}\nabla^2 V, \quad (14)$$

where V is the velocity vector and P is the pressure. Fluent ver. 6.3 proprietary solver is employed to solve equation (13) and equation (14). It has been well validated for simulating

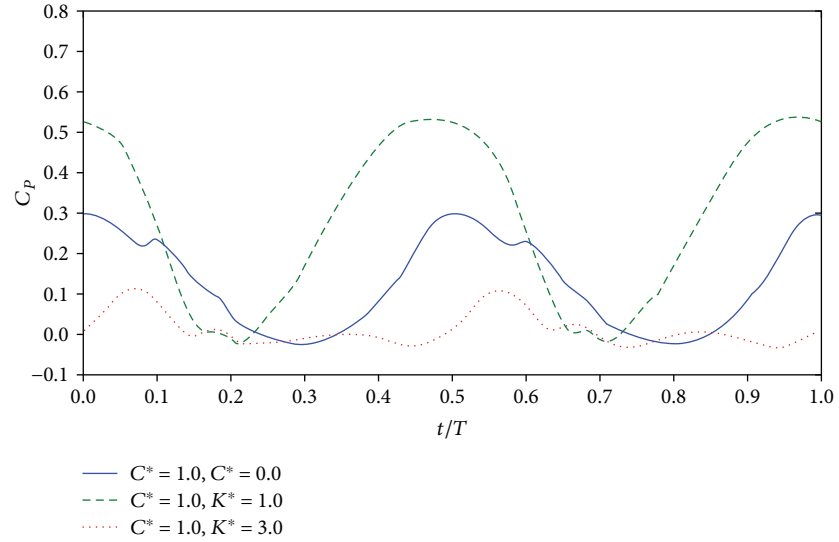

Figure 6: The time variation of power coefficient of the considered cases with $C^* = 1.0$ and $K^* = 0.0$, 1.0, and 3.0.

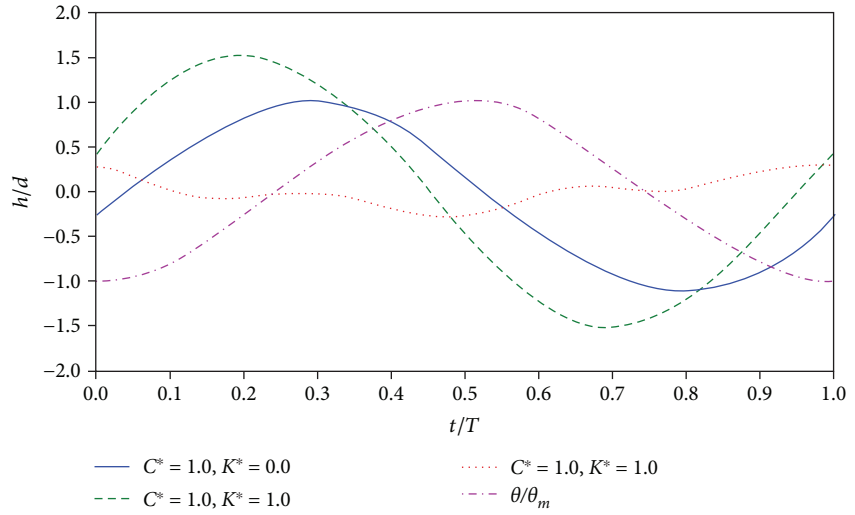

Figure 7: The time variation of h/d of the considered cases with $K^* = 0.0$, 1.0, and 3.0, $C^* = 1.0$.

flapping wing problems [15, 16]. The second-order upwind algorithm is adopted for the space discretization, and first-order implicit algorithm is selected for time discretization. Meanwhile, SIMPLE algorithm is selected for solving the coupling between the pressure and the velocity. The convergence criterion for the solver is satisfied with residual less than 10^{-3}.

Finite Center Difference method is employed to solve passive plunging motion governing equation (3), which is embedded in Fluent ver. 6.3 by using a user-defined function (UDF). Dynamic mesh technique is also employed to update the wing's position (active pitching and passive plunging) at each time step. For more details about the coupling method to solve interaction of fluid and the semiactive flapping wing, one can refer to our previous work [5, 17].

The computational domain of this work has C type shape. According to the works of Zhu and Peng [18], the

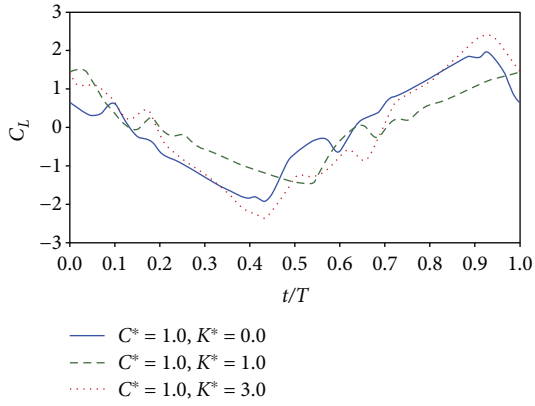

Figure 8: The time variation of lift coefficient of the considered cases with $K^* = 0.0$, 1.0, and 3.0, $C^* = 1.0$.

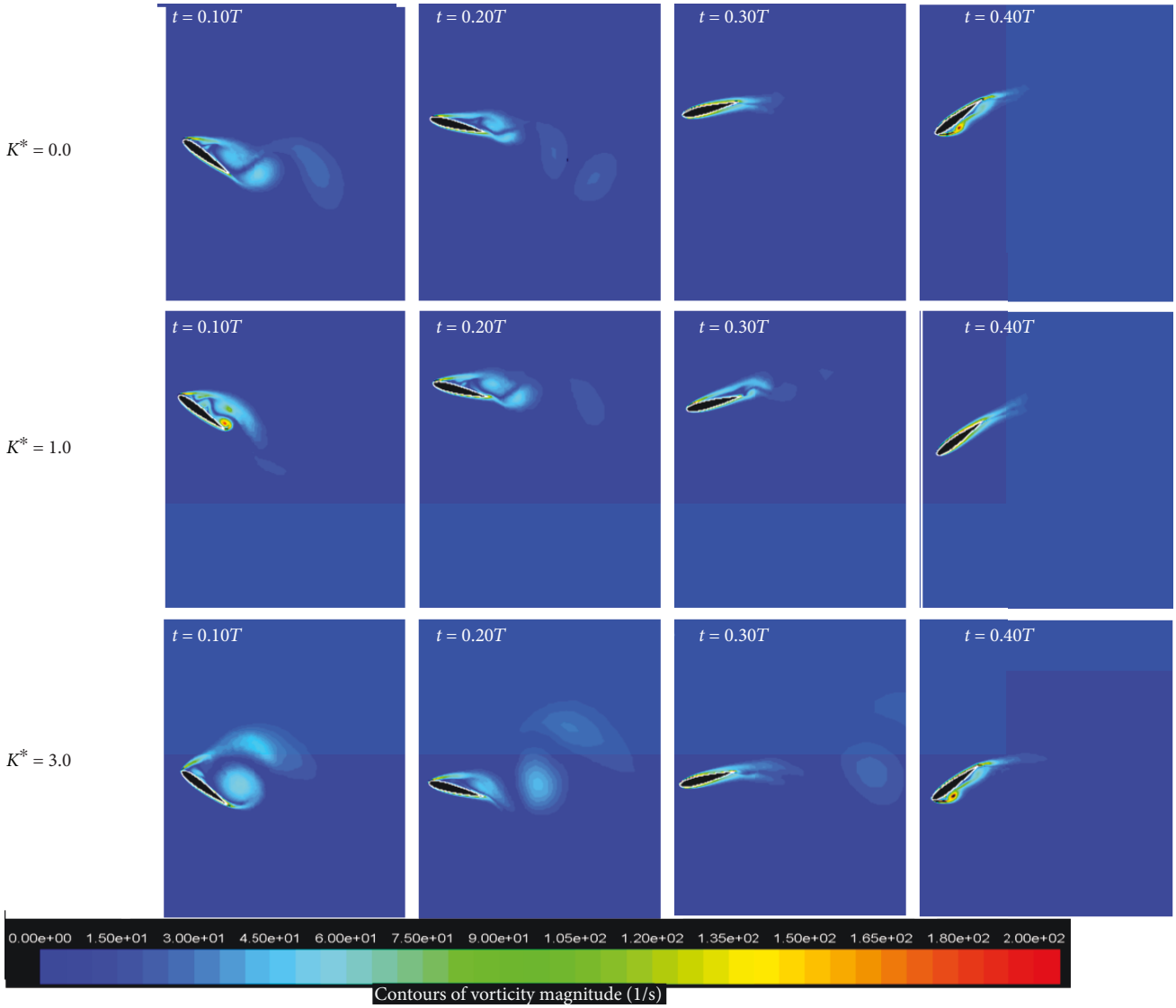

Figure 9: The vorticity contours of the considered cases with $K^* = 0.0$, 1.0, and 3.0, $C^* = 1.0$.

distance between the outer boundary and the airfoil is at about $8d$ lengths; flow field and the aerodynamic performance of the semiactive flapping airfoil are not significant by the far field boundary. Therefore, the radius of the semicircle on the left side of the computational domain is fixed $20d$, and the size of the rectangle on the right side of the computational domain is set as $L = 20d$, $H = 40d$. A triangular mesh system is employed where a C type computational domain (shown in Figure 2) containing an inner flapping domain and an outer fixed domain, and the inner domain which moves according to the wing kinematics, and the first grid is located at $0.001c$ from the wing surface, the growth rate of the grid size is 1.08.

The no-slip wall boundary condition is applied at the semiactive flapping wing. The inlet velocity defined as $u = U_\infty$ is imposed on the left, up, and low side of the domain. Pressure-outlet boundary condition which has zero static pressure is imposed on the right side of the domain.

2.3. Validation. To validate the independence of the numerical results on the special-discretization and time-discretization scheme, computations with different meshes and iteration time steps are simulated. These checks are carried out on the representative case of $\theta_m = 45°$, $f^* = 0.32$, $\mathrm{Re} = 3400$, $C^* = 2.00$, $K^* = 1.0$, and $M^* = 60$. The power coefficient calculated by the coarse mesh (the first grid is located at $0.005c$ from the wing surface, the growth rate of the grid size is 1.08, total 4.22×10^4 cells), medium mesh (the first grid is located at $0.001c$ from the wing surface, the growth rate of the grid size is 1.08, total 8.39×10^4 cells), and fine mesh (the first grid is located at $0.0005c$ from the wing surface, the growth rate of the grid size is 1.08, total 1.51×10^5 cells) with iteration time steps $\Delta t = T/2000$ and $\Delta t = T/4000$ is shown in Figure 3. It is seen from this figure that the meshes and time steps have slightly influenced the computation results. Therefore, the medium mesh is sufficiently dense and iteration time steps $\Delta t = T/2000$ is

sufficiently small to grasp the main flow features over the wing, and they are employed for the next simulations.

To validate the coupling method for the study on the semiactive flapping wing, a typical case of a semiactive flapping wing (wing shape is also NACA0015) which was numerical studied by Teng et al. [19] is simulated. The simulation parameters are set the same as the parameters used by Teng et al. [19]: Re = 1000, $\theta_m = 45^\circ$ and $f^* = 0.16$, $C^* = \pi$, $K^* = 0.0$, and $M = 1.0$ kg. The resulting lift coefficient $(C_L = F_L/(0.5\rho U_\infty{}^2 d))$ of the wing is plotted against time as shown in Figure 4. Comparing to the result by Teng et al. [19], good agreement is achieved.

3. Results and Discussions

As conducted above, the main parameters were related to the response of the semiactive flapping wing including the pitching amplitude θ_m, reduced frequency f^*, Reynolds number Re, damping coefficient C^*, spring coefficient K^*, and mass ratio M^*. To simplify the problem, the factor θ_m is fixed at 45°, f^* is set at 0.32, and Re keeps a value of 3.4×10^3. Consequently, the key parameters that affect the power extraction performance of the semiactive flapping wing are the damping coefficient C^*, spring coefficient K^*, and mass ratio M^*. The details of these three parameters studied in this paper are summarized in Table 1. Note that the parameter spaces in this work are almost covering all the parameters studied in the literature as discussed in Introduction, but some controversial conclusions are conducted; therefore, it needs to be studied further.

3.1. Effect of Damping Coefficients and Spring Coefficients. To examine the effect of damping and spring coefficient, the mass ratio M^* is fixed at 60 first. Figure 5 plots the mean power coefficient and power efficiency against spring coefficient K^* with different damping coefficient C^*. Obviously, in this figure that at a given C^* both mean power coefficient and power efficiency increase first then decrease and achieve a maximum at $K^* = 1.0$. However, when K^* is larger than 1.0, both mean power coefficient and power efficiency of the wing decrease sharply, which implies the power extraction performance of the wing is deteriorated. In addition, for $K^* = 1.0$, the maximum mean power coefficient of the wing monotonically decrease with C^*, while the maximum power efficiency of the wing increase first then decrease and achieve a maximum at $C^* = 4.0$. This conclusion is different with the results obtained by Zhu et al. [12], at which they concluded that the best power extraction performance of the wing is achieved, when the spring coefficient is at 0.00 and the damping coefficient is at a value of π. These difference can be due to the potential flow theory used by Zhu et al. [12], for which the viscosity effect and the interaction between wing and vortex are neglected.

To explore the mechanism of how the spring coefficients and damping coefficients influence the power extraction performance of the semiactive flapping wing in detail, we first investigate the performance of the wing with fixed $C^* = 1.0$, and three typical cases with $K^* = 0.0$, 1.0, and 3.0 are studied. The time variation of power coefficient of the above considered cases is shown in Figure 6. It is clear in this figure that the wing with $K^* = 1.0$ has the largest power coefficient amplitude, then is the wing with $K^* = 0.00$, and the wing with $K^* = 3.0$ has the smallest power coefficient amplitude, which is consistent with the mean power generation of the wing as shown in Figure 5. Meanwhile, there exists phase difference between the three wings. The wing with $K^* = 1.0$

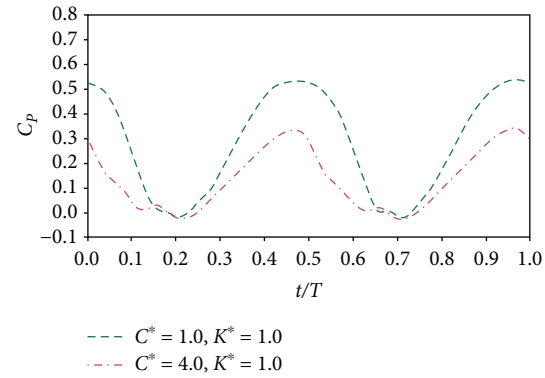

Figure 10: The time variation of power coefficient of the considered cases with $K^* = 1.0$, $C^* = 1.0$ and 4.0.

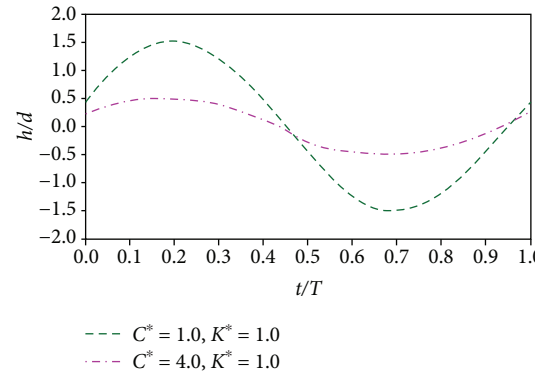

Figure 11: The time variation of h/d of the considered cases with $C^* = 1.0$ and 4.0, $K^* = 1.0$.

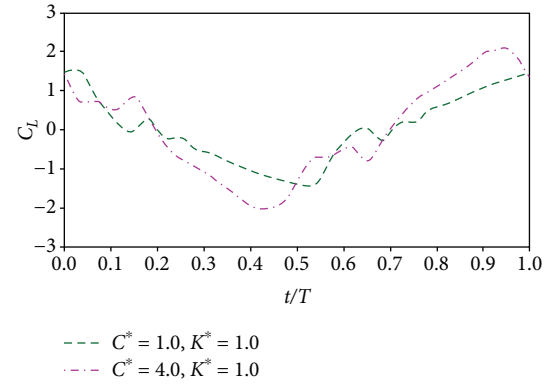

Figure 12: The time variation of lift coefficient of the considered cases with $C^* = 1.0$ and 4.0, $K^* = 1.0$.

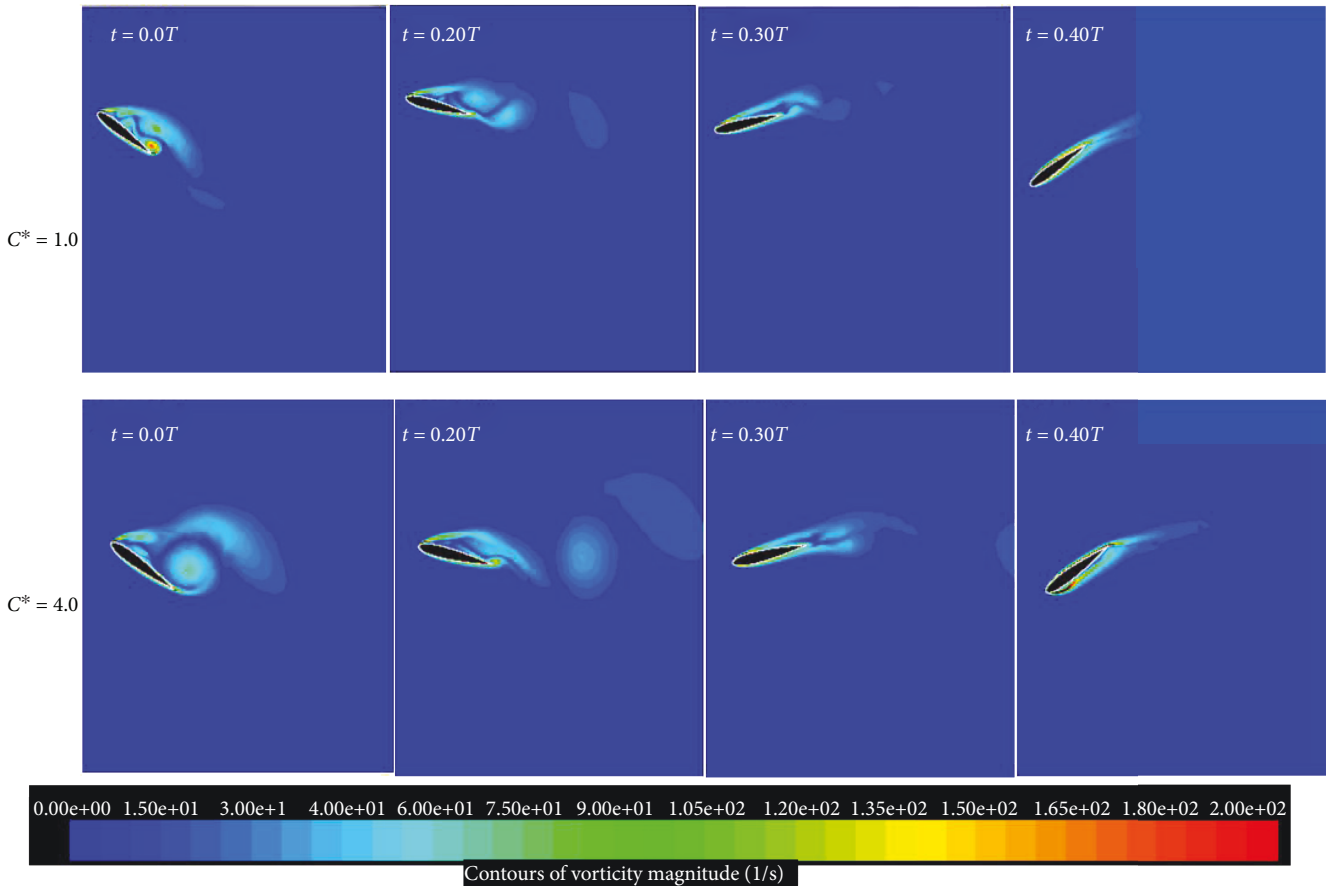

Figure 13: The vorticity contours of the considered cases with $C^* = 1.0$ and 4.0, $K^* = 1.0$.

has the earliest time to achieve maximum power coefficient, then is the wing with $K^* = 0.00$, and the wing with $K^* = 3.0$ has the latest to achieve maximum power coefficient.

Besides the power coefficient, the power efficiency of the wing is also influenced by the plunging motion $h(t)$. Figure 7 shows the time variation of $h(t)$ of the above three considered cases, where the defined pitching motion $\theta(t)$ is also illustrated for comparison. It is found from this figure that the amplitude of the $h(t)$ first increase then decrease with K^*, and the phase difference between pitching and $h(t)$ is -0.305T, -0.205T, and 0.475T for the wing with $K^* = 0.0$, 1.0, and 3.0, respectively. Moreover, nonharmonic time variation of $h(t)$ is observed for the wing with $K^* =$ 3.0, which indicates the complex lift force induced by the wing with $K^* = 3.0$.

Figure 8 shows the time variation of lift coefficient $(C_L = F_L/(0.5\rho U_\infty{}^2 d))$ of the above three considered cases. It is seen from this figure that different with the time variation of $h(t)$, the amplitude of the C_L first decrease then increase with K^*. The wing with larger amplitude of C_L has smaller amplitude of $h(t)$.

To explore the physical mechanism of the effect of variation of spring coefficient, Figure 9 shows the vorticity contours during a semipitching cycle ($t = 0.10T$-$0.40T$). Due to the symmetrical flapping of the wing, semipitching cycle is considered. It is seen from this figure that the spring coefficient can influence the vortex structure of the wing significantly. Comparing with the wing with $K^* = 0.0$, there are less separated vortex in the wake for the wing with $K^* = 1.0$, and the separated vortex can reattach to the wing surface during flapping; moreover, there are weaker leading edge vortex generating for the wing with $K^* = 1.0$, which results the wing to have smaller lift coefficient as shown in Figure 8. Moreover, the separated vortex in the wake indicates more power disappeared, which is the reason why the wing with $K^* = 1.0$ has larger mean power coefficient and efficiency. On the other hand, for the wing with $K^* = 3.0$, obviously, there are more separated vortex in the wake comparing with the wing with $K^* = 0.0$; however, the stronger leading edge vortex are generated by the wing with $K^* = 3.0$, which is the reason why the wing with $K^* = 3.0$ has larger lift coefficient but smaller mean power coefficient and efficiency.

After investigating the effect of spring coefficient on the power extraction performance of the semiactive flapping wing, the effect of damping coefficient on the power extraction performance of the semiactive flapping wing is studied. To this end, we study the performance of the wing with fixed $K^* = 1.0$, and two typical cases with $C^* = 1.0$ and 4.0 are investigated in details. The time variation of power coefficient of the above considered cases is shown in Figure 10. It is clear in this figure that the wing with $C^* = 1.0$ has the larger power coefficient than the wing with $C^* = 4.0$ almost during

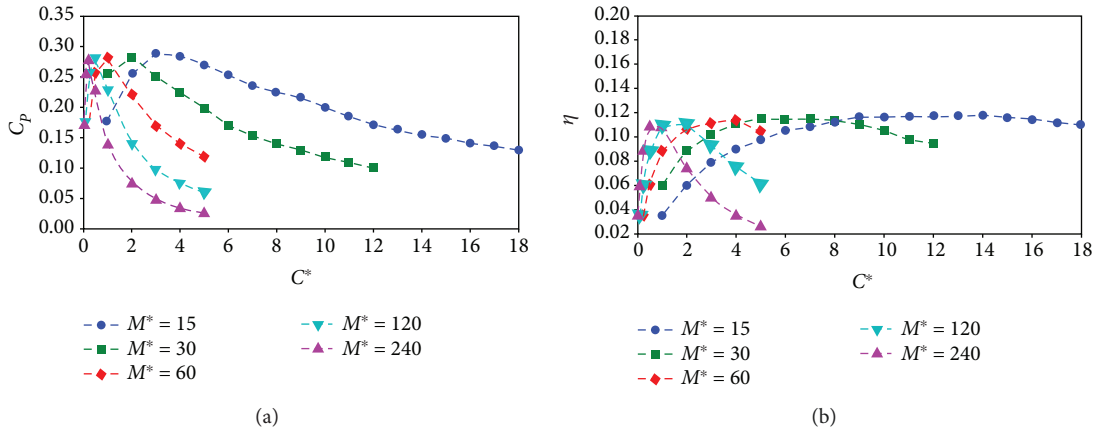

FIGURE 14: The mean power coefficient and power efficiency against damping coefficient C^* with different mass ratio M^*; (a) mean power coefficient; (b) power efficiency.

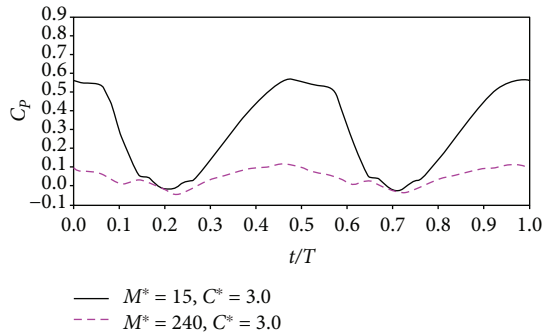

FIGURE 15: The time variation of power coefficient of the considered cases with $M^* = 15$, $C^* = 3.0$ and $M^* = 240$, $C^* = 3.0$.

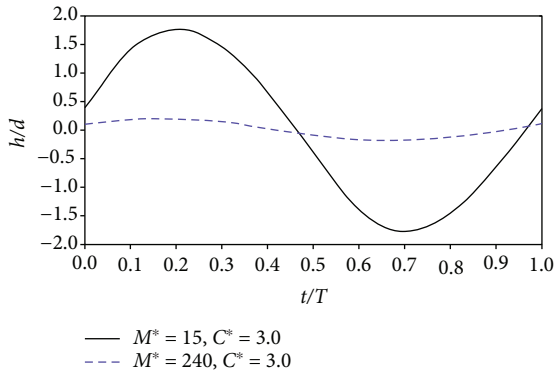

FIGURE 16: The time variation of h_{max}/d of the considered cases with $M^* = 15$, $C^* = 3.0$ and $M^* = 240$, $C^* = 3.0$.

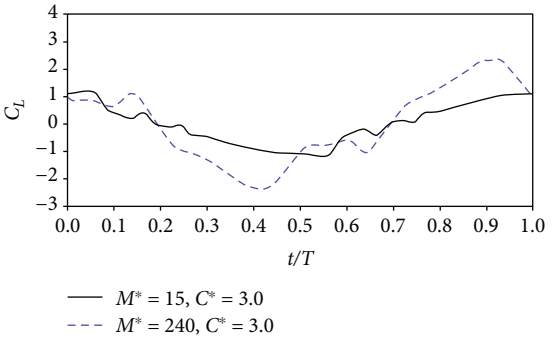

FIGURE 17: The time variation of lift coefficient ($C_L = F_L/(0.5\rho U_\infty{}^2 d)$) of the considered cases with $M^* = 15$, $C^* = 3.0$ and $M^* = 240$, $C^* = 3.0$.

the whole flapping cycle, which is consistent with the mean power generation of the wing as shown in Figure 5.

Figure 11 shows the time variation of $h(t)$ of the above two considered cases. The same as the power coefficient, the amplitude of the $h(t)$ of the wing with $C^* = 1.0$ has larger amplitude than the wing with $C^* = 4.0$; however, comparing with the pitching motion, the two considered wings have almost identical phase difference.

Figure 12 shows the time variation of lift coefficient of the two considered wings with $C^* = 1.0$ and 4.0, $K^* = 1.0$. It is seen from this figure that contrary with the time variation of $h(t)$, the wing with $C^* = 4.0$ has larger amplitude of lift coefficient than the wing with $C^* = 1.0$.

Figure 13 shows the vorticity contours of the two considered wings with $C^* = 1.0$ and 4.0, $K^* = 1.0$ during a semi-pitching cycle. Obviously, in this figure, there exists a vortex separated for the wing with $C^* = 4.0$ (see $t = 0.20T$), while for the wing with $C^* = 1.0$, no obviously separated vortex is observed, which results that the wing with $C^* = 4.0$ has smaller mean power coefficient. It is also found that the passive plunging amplitude of the wing with $C^* = 1.0$ has larger value than the wing with $C^* = 4.0$. According to equation (11), when the increased passive plunging amplitude of the wing is larger than the increased mean power coefficient, the efficiency of the wing will fall. This is the reason why the wing with $C^* = 4.0$ has smaller mean power coefficient but has larger power efficiency.

3.2. Effect of Mass Ratio. To examine the effect of mass ratio, the spring coefficient K^* is fixed at 1.00, which has the best energy extraction performance under different damping coefficient as section above discussed.

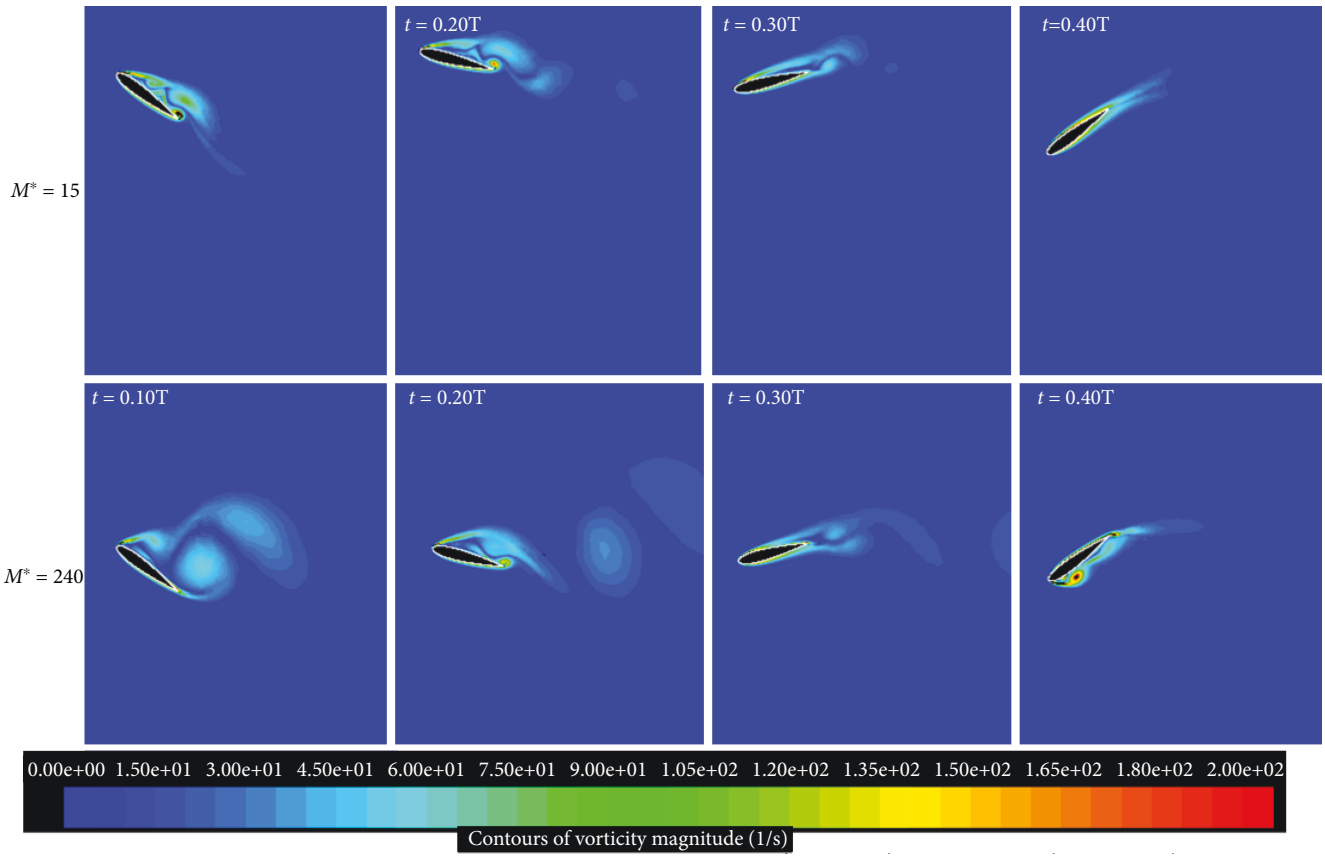

Figure 18: The vorticity contours of the considered cases with $M^* = 15$, $C^* = 3.0$ and $M^* = 240$, $C^* = 3.0$.

Figure 14 plots the mean power coefficient and power efficiency against damping coefficient C^* with different mass ratio M^*. There are three interesting conclusions that can be concluded from this figure. Firstly, at a given M^*, both mean power coefficient and power efficiency increase first then decrease; moreover, the value of C^* at which the wing achieves maximum mean power coefficient is smaller than the wing at which achieves maximum power efficiency. Secondly, the maximum mean power coefficient and power efficiency, respectively, are almost identical for the wing with different M^*; however, the value of C^* at which the wing achieves the maximum mean power coefficient and power efficiency decreases with M^* increasing. Thirdly, for the wing with smaller M^*, both the mean power coefficient and power efficiency are insensitive to the variation of damping coefficient $C^*(C^* = 5\sim18)$, which indicates that the wing with smaller M^* has better working stability that, therefore, leads the wing to have better power extraction performance.

To explore the mechanism of how the mass ratio influence the power extraction performance of the semiactive flapping wing in detail, two typical cases with $M^* = 15$, $C^* = 3.0$ and $M^* = 240$, $C^* = 3.0$ are considered. Figure 15 shows the time variation of power coefficient of the above two considered cases. It is clear in this figure that for the wing with $M^* = 15$, $C^* = 3.0$, it has larger power coefficient than the wing with $M^* = 240$, $C^* = 3.0$ almost the whole pitching cycle, and it also has earlier time to achieve maximum power coefficient.

Figure 16 shows the time variation of h/d of the above two considered cases. The wing with $M^* = 15$, $C^* = 3.0$, has larger amplitude of h/d than the wing with $M^* = 240$, $C^* = 3.0$; meanwhile, the phase difference between pitching and h of the two considered wings is identical; the value is $0.30T$.

Figure 17 shows the time variation of lift coefficient $(C_L = F_L/(0.5\rho {U_\infty}^2 d))$ of the above two relation cases. Different from the time variation of power coefficient and the passive plunging motion h, the wing with $M^* = 15$, $C^* = 3.0$, has smaller amplitude of lift coefficient than the wing with $M^* = 240$, $C^* = 3.0$; meanwhile, comparing to the wing with $M^* = 240$, $C^* = 3.0$, there exists an obvious phase delay for the wing with $M^* = 15$, $C^* = 3.0$, to achieve maximum lift coefficient.

Figure 18 shows four instantaneous vorticity contours of the above considered wings during a semipitching cycle. It is seen from this figure that the mass ratio can influence the flow field of the wing significantly. Similar as the wing with different damping coefficient (as shown in Figure 13), there exists a vortex separated for the wing with $M^* = 240$ (see $t = 0.10T$ to $0.30T$), while for the wing with $M^* = 15$, no obviously separated vortex is observed, which results the wing with $M^* = 240$ has smaller mean power coefficient. It is also found that the passive plunging amplitude of the wing with $M^* = 15$ has larger value than the wing with $M^* = 240$. According to equation (11), when the increased passive plunging amplitude of the wing is larger than the increased

mean power coefficient, the efficiency of the wing will fall. This is the reason why the wing with $M^* = 240$ has smaller mean power coefficient but has larger power efficiency.

4. Conclusion

In this paper, the power extraction performance of the semiactivated flapping wing with different damping coefficient, spring coefficient, and mass ratio is numerically examined. A numerical code based on Finite Volume method to solve the two-dimensional Navier-Stokes equations and coupled with Finite Center Difference method to solve passive plunging motion equation is developed.

We first examine the effect of damping coefficient and spring coefficient and fix the mass ratio at 60. It is found that an optimal set of spring coefficient ($K^* = 1.00$) is obtained, for which both the high mean power coefficient and power efficiency are achieved no matter what the damping coefficient value of the wing is. Second, the effect of mass ratio is examined, and the spring coefficient is fixed at 1.00. It is concluded that the variation of mass ratio cannot increase the maximum mean power coefficient and power efficiency of the semiactivated flapping wing, but it can influence the value of damping coefficient C^* at which the wing achieves the maximum mean power coefficient and power efficiency; moreover, insensitivity of the mean power coefficient and power efficiency to the variation of damping coefficient C^* is observed for the wing with smaller mass ratio, which indicates that the wing with smaller M^* has better working stability. More specifically, the flow field around the wing is also investigated, and for the wing with appropriate damping coefficient, spring coefficient, and mass ratio ($K^* = 1.00$, $C^* = 4.0$, and $M^* = 60$), the separated vortex can reattach to the wing surface during flapping, which results in no obvious vortex disappeared in the wake. This is the reason for the wing to have better power extraction performance.

Notations

d: Chord length of wing
M: Mass of the airfoil
C: Damping coefficient
K: Spring constant
$\theta(t)$: Pitching motion
$h(t)$: Passive plunging motion
θ_m: Pitching amplitude
f: Pitching frequency
T: The pitching period
F_L: The lift force
C^*: Damping coefficient
K^*: Spring coefficient
M^*: Mass ratio
ρ: Fluid density
ρ_s: The wing density
S: Area of the wing
Re: Reynolds number
U_∞: The stream velocity
μ: The fluid kinematic viscosity
f^*: Reduced frequency
P_E: The power extracted from the fluid
P_I: The power needed to input the system
M_T: The fluid torque
ω: The pitching velocity
$\dot{h}$: The passive plunging velocity
P_T: The net power
C_P, $\overline{C_P}$: The power coefficient and mean power coefficient
η: The power extraction efficiency
$h_{\max}$: The overall vertical extent of the wing motion
V: The velocity vector
P: The pressure.

Data Availability

The data used to support the findings of this study are included within the article.

Conflicts of Interest

The authors declare that they have no conflict of interest.

Acknowledgments

This study was funded by the National Natural Science Foundation of China (project No. 51505347) and Key Laboratory of Metallurgical Equipment and Control of Education Ministry, Wuhan University of Science and Technology Foundation (2015B07).

References

[1] A. B. Rostami and M. Armandei, "Renewable energy harvesting by vortex-induced motions: review and benchmarking of technologies," *Renewable & Sustainable Energy Reviews*, vol. 70, pp. 193–214, 2017.

[2] J. Young, J. C. S. Lai, and M. F. Platzer, "A review of progress and challenges in flapping foil power generation," *Progress in Aerospace Sciences*, vol. 67, pp. 2–28, 2014.

[3] M. Pourmahdavi, M. N. Safari, and S. Derakhshan, "Numerical investigation of the power extraction mechanism of flapping foil tidal energy harvesting devices," *Energy & Environment*, vol. 30, no. article 0958305X1878732, pp. 193–211, 2019.

[4] A. Javed, M. Jamil, B. Ali, K. Djidjeli, and T. A. Shams, "Performance analysis of flapping foil flow energy harvester subjected to non-sinusoidal pitching motion," in *2018 Fluid Dynamics Conference*, Atlanta, GA, USA, 2018.

[5] J. Zhu and T. Tian, "The time asymmetric pitching effects on the energy extraction performance of a semi-active flapping wing power generator," *European Journal of Mechanics - B/Fluids*, vol. 66, pp. 92–101, 2017.

[6] W. Mckinney and J. Delaurier, "Wingmill: an oscillating-wing windmill," *Journal of Energy*, vol. 5, no. 2, 115 pages, 1981.

[7] Q. Zhu, "Optimal frequency for flow energy harvesting of a flapping foil," *Journal of Fluid Mechanics*, vol. 675, no. 675, pp. 495–517, 2011.

[8] Q. Xiao and Q. Zhu, "A review on flow energy harvesters based on flapping foils," *Journal of Fluids and Structures*, vol. 46, no. 2, pp. 174–191, 2014.

[9] J. Wu, Y. L. Chen, and N. Zhao, "Role of induced vortex interaction in a semi-active flapping foil based energy harvester," *Physics of Fluids*, vol. 27, no. 9, article 093601, 2015.

[10] J. Wu, Y. L. Qiu, C. Shu, and N. Zhao, "Pitching-motion-activated flapping foil near solid walls for power extraction: a numerical investigation," *Physics of Fluids*, vol. 26, no. 8, article 83601, 2014.

[11] J. Zhan, B. Xu, J. Wu, and J. Wu, "Power extraction performance of a semi-activated flapping foil in gusty flow," *Journal of Bionic Engineering*, vol. 14, no. 1, pp. 99–110, 2017.

[12] Q. Zhu, M. Haase, and C. H. Wu, "Modeling the capacity of a novel flow-energy harvester," *Applied Mathematical Modelling*, vol. 33, no. 5, pp. 2207–2217, 2009.

[13] J. Deng, L. Teng, D. Pan, and X. Shao, "Inertial effects of the semi-passive flapping foil on its energy extraction efficiency," *Physics of Fluids*, vol. 27, no. 5, pp. 53103–53191, 2015.

[14] H. Abiru and A. Yoshitake, "Study on a flapping wing hydroelectric power generation system," *Journal of Environment and Engineering*, vol. 6, no. 1, pp. 178–186, 2011.

[15] M. A. Ashraf, J. Young, and J. C. S. Lai, "Reynolds number, thickness and camber effects on flapping airfoil propulsion," *Journal of Fluids and Structures*, vol. 27, no. 2, pp. 145–160, 2011.

[16] F. M. Bos, D. Lentink, B. W. van Oudheusden, and H. Bijl, "Influence of wing kinematics on aerodynamic performance in hovering insect flight," *Journal of Fluid Mechanics*, vol. 594, pp. 341–368, 2008.

[17] Z. Jianyang, J. Lin, and H. Yu, "Aerodynamic performance of the three-dimensional lumped flexibility bionic hovering wing," *International Journal of Aerospace Engineering*, vol. 2018, Article ID 1314258, 14 pages, 2018.

[18] Q. Zhu and Z. Peng, "Mode coupling and flow energy harvesting by a flapping foil," *Physics of Fluids*, vol. 21, no. 3, article 033601, 2009.

[19] L. Teng, J. Deng, D. Pan, and X. Shao, "Effects of non-sinusoidal pitching motion on energy extraction performance of a semi-active flapping foil," *Renewable Energy*, vol. 85, pp. 810–818, 2016.